Barriers of Hydrogen Abstraction from Primary, Secondary, and Tertiary Alkane Sites by O(^{3}P)

Diego Troya

Department of Chemistry, Virginia Tech, 107 Davidson Hall, Blacksburg, Virginia 24061-0212

Received: July 3, 2007; In Final Form: August 15, 2007

We present an extensive study of the barriers of hydrogen abstraction from primary, secondary, and tertiary sites of acyclic alkanes by ground-state oxygen atoms. Our studies include the characterization of the lowest-energy transition states of the O(^{3}P) reactions with methane, ethane, propane, isobutane, and isopentane using high-level ab initio methods. The order of the calculated barriers heights is primary > secondary > tertiary, in agreement with the trends gleaned from kinetic measurements. Analysis of the transition-state geometry reveals a shift toward more reagents-like structures in the primary → secondary → tertiary sequence, which concurs with the expectation from Hammond's postulate. Using the ab initio data, we calculate thermal rate constants via transition-state theory. Our highest-level calculations indicate that the room-temperature relative reactivities of primary, secondary, and tertiary alkane sites in hydrogen-abstraction reactions by ground-state oxygen atoms are 1, 29, and 422, respectively. These results are used to interpret recent experiments on the reactions of O(^{3}P) with liquid alkanes.

I. Introduction

Almost 40 years ago, thermal rate constant measurements of O(^{3}P) + alkane → OH + alkyl reactions indicated that the activation energy of these hydrogen-abstraction processes depended on the type of C−H bond involved in the reaction.[1] O(^{3}P) reactions with alkanes possessing primary, secondary, or tertiary hydrogen-abstraction sites had widely different thermal rate constants. These measurements permitted one to infer that the activation energies are in the primary > secondary > tertiary order, in agreement with the dissociation energies of the corresponding C−H bonds. These results were also in line with one of the most common interpretations of Hammond's postulate:[2] a factor stabilizing a reaction intermediate also stabilizes the transition state leading to that intermediate. Since the exothermicity of a O + alkane hydrogen-abstraction reaction at a tertiary site is larger than at secondary and primary sites, Hammond's postulate predicts that barriers for reaction at tertiary sites should be smaller than those at secondary and primary sites.

The trend that the reaction barrier of the O(^{3}P) + alkane reactions follows the primary > secondary > tertiary order has since been invoked in a variety of experiments concerning the dynamics of these reactions. Andresen and Luntz measured that the yield of OH(v'=1) depended strongly on the type of hydrogen atom being abstracted.[3] Thus, while in reactions involving only primary hydrogen atoms the OH(v'=1):OH(v'=0) ratio was measured to be 0.01, it increased to 0.24 for reactions with only secondary hydrogen atoms and to 1.4 for reactions involving tertiary hydrogen atoms. Drawing inspiration from the early rate-constants measurements, these results were interpreted to emerge from a change in the potential-energy surface of the O(^{3}P) + alkane reactions, which becomes more attractive and has a smaller barrier as one moves from primary to secondary and tertiary sites and promotes OH vibrational excitation in that same order. Later, measurements of OH vibrational excitation in O + alkane reactions by the group of McKendrick[4,5] borne out the earlier findings of Andresen and Luntz.

Very recently, the work by the groups of Minton[6−8] and McKendrick[9−11] on the reaction of O(^{3}P) with liquid-saturated hydrocarbons has renewed interest in understanding the different reactivity and dynamics of primary, secondary, and tertiary sites in these molecules. In particular, the set of experiments by McKendrick has probed the reactions of O(^{3}P) with squalane (2,6,10,15,19,23-hexamethyltetracosane, $C_{30}H_{62}$), an acyclic alkane containing primary, secondary, and tertiary sites, by measuring the internal-state distribution of the OH product. One of the experimental findings is that a fraction of the OH product emerges vibrationally excited from the reaction. Comparison of these gas/surface results with the gas-phase O + alkane measurements of OH vibrational excitation mentioned above suggests that vibrational excitation in the gas/surface collisions originates from reactions occurring at secondary and possibly tertiary sites.

To shed light into the possibility that sites other than primary participate in the O + squalane reaction, the group of McKendrick carried out molecular dynamics simulations of the structure of the gas/liquid interface of squalane.[12] The simulations revealed that although primary sites are predominant at the surface of squalane, collisions of O(^{3}P) with secondary and tertiary sites are also possible. The ∼10% population in OH(v'=1) measured by that group in O(^{3}P) + squalane collisions was therefore tentatively attributed to reactions occurring at secondary and tertiary sites of the liquid alkane. Although those molecular dynamics simulations have provided qualitative insight into the microscopic origin of vibrational excitation in the OH product of the O + squalane reaction, the independent contribution of primary, secondary, and tertiary sites to the total OH yield has not been quantified yet.

In this paper, we use electronic structure calculations in combination with transition-state theory to quantify the relative reactivity of primary, secondary, and tertiary alkane sites in

10.1021/jp075174i CCC: $37.00
Published on Web 10/03/2007

TABLE 1: Calculated Reaction Energy and Barrier (kcal/mol) of the O + CH_4 → OH + CH_3 Reaction

method	$\Delta H^{\ddagger}$ [a]	$\Delta E^{\ddagger}$ [b]	$\Delta_r H$ [c]	$\Delta_r E$ [d]
CCSD(T)/CBS//B3LYP/adz	10.56	14.13	1.23	5.11
CCSD(T)/CBS//B3LYP/atz	10.54	14.14	1.06	5.09
CCSD(T)/CBS//MP2/adz	10.07	14.10	1.11	5.03
CCSD(T)/CBS//MP2/atz	10.29	14.19	0.98	5.07
MP2/CBS//MP2/adz	12.71	16.74	0.24	4.16
PMP2/CBS//MP2/adz	9.90	13.93	−1.13	2.79
MP4/CBS//MP2/adz	11.40	14.43	1.37	5.29
PMP4/CBS//MP2/adz	9.79	13.82	0.62	4.54
B3LYP/CBS//MP2/adz	4.10	8.13	−1.39	2.52
CASPT2/CBS[e]//CASPT2/tz	7.9	12.6	−0.1	4.1
MRCI+Q/CBS[e]//CASPT2/tz	10.5	15.2	1.4	5.6
exp[23] (0 K)			1.6 ± 0.2	
exp[23] (298 K)			2.2 ± 0.2	
exp[24] (298 K)			2.2 ± 0.3	
exp[25] (298 K)			2.2	
exp[26] (298 K)			2.5	

[a] Zero-point corrected transition-state energy referred to reagents. [b] Classical, i.e., not zero-point corrected transition-state energy referred to reagents. [c] Zero-point corrected reaction energy. [d] Classical, i.e., not zero-point corrected reaction energy. [e] The extrapolation to the basis set limit has been performed with the cc-pVTZ and cc-pVQZ basis sets, i.e., without including diffuse functions, ref 20.

abstraction reactions with ground-state atomic oxygen. Our goal is to produce accurate relative reaction rates that can aid in deciphering the dynamics of O-atom reactions at a hydrocarbon surface. To this end, we present calculations of reaction barriers and thermal rate constants of hydrogen abstraction by O(^{3}P) from benchmark gas-phase alkane molecules including primary, secondary, and tertiary sites. A second goal in this paper is to verify using computational methods the validity of the often-invoked Hammond's postulate for O(^{3}P) + alkane reactions. As mentioned above, this postulate suggests that the hydrogen abstraction at tertiary sites should possess the lowest barrier, as it is the most exothermic process. It also suggests that the geometry of the transition state for abstraction at tertiary sites should resemble reagents more closely than the transition states for abstraction at secondary and primary sites.

II. Computational Details

We have calculated the energies and barriers of the hydrogen-abstraction reactions between O(^{3}P) and methane (CH_4), ethane (C_2H_6), propane (C_3H_8), isobutane (i-C_4H_{10}), and isopentane (i-C_5H_{12}) using electronic structure methods. Geometry optimizations and harmonic frequency calculations of reagents, products, and transition-state structures have been carried out mainly using second-order Möller−Plesset perturbation theory (MP2) with the correlation-consistent double-ζ basis set of Dunning augmented with diffuse functions (aug-cc-pVDZ). Utilizing the geometries and harmonic frequencies at that level, single-point energy calculations have been carried out with the MP2 method and the larger aug-cc-pVTZ and aug-cc-pVQZ basis sets. (In the tables, we replace the aug-cc-pV*N*Z notation by a*n*z, where *N* (*n*) is D (d), T (t), or Q (q)). In addition, for the smaller systems (O + methane, ethane, and propane) dual-level coupled-cluster calculations with single, double, and perturbative triple excitations (CCSD(T)) have been used to obtain a higher-level estimate of the reaction energies and barriers. Fourth-order Möller−Plesset perturbation theory (MP4) and density functional theory (B3LYP functional) have also been used for O(^{3}P) + CH_4. Extrapolations to the complete basis-set limit have been performed from the dual-level calculations with the aug-cc-pVTZ and aug-cc-pVQZ basis sets employing a two-point extrapolation procedure.[13] Most of the electronic structure calculations have been conducted using the Gaussian03 program suite.[14] Some of the single-point CCSD(T) evaluations been carried out with the PSI3 program.[15]

All of the calculations involving open-shell species have been computed using an unrestricted reference. The transition states of the O + methane and O + ethane reactions, and some of the transitions states in O + propane and O + isobutane possess C_s symmetry. In these transition states, the results refer to the lowest-energy ^{3}A″ state. In nonsymmetric systems, the calculations refer to the lowest-energy triplet state.

The calculations have been carried out at 0 K. In an effort to establish the accuracy of our study, we compare our calculated reaction energies with experimental values for O + CH_4 and O + C_2H_6. Most of the experimental reaction energies have been obtained from the heats of formation of the product and reagent species at 298 K. Therefore, quantitative comparison between theoretical and experimental reaction energy requires a 0→298 K thermal correction. This correction makes the reactions at 298 K approximately 0.5 kcal/mol less exothermic than at 0 K.

III. Results

(a) O(^{3}P) + Methane. The O(^{3}P) + CH_4 → OH + CH_3 reaction is the simplest O + alkane hydrogen-abstraction reaction. Due to the relatively low number of electrons involved in the reaction, the reaction energetics have been heavily studied before with a plethora of electronic structure methods.[16−21] (See ref 5 for a review.) The highest-level calculations of the transition state available to date correspond to multireference configuration-interaction (MRCI) data extrapolated to the complete basis-set limit (CBS).[20] Here we use these earlier high-accuracy calculations as a benchmark to calibrate the performance of lower-cost methods that we have used to calculate the energetics of larger O + alkane reactions. This calibration is important because MRCI calculations quickly become prohibitive for O(^{3}P) + alkane reactions beyond O + CH_4 and O + C_2H_6.

Table 1 shows a comparison of the reaction energies and barriers determined with a variety of electronic structure methods. Both the reaction energy and barrier calculated at the CCSD(T)/CBS level are within 0.5 kcal/mol of the MRCI/CBS data of ref 20, indicating that CCSD(T) is an accurate method for this reaction, including the transition-state region. Much as was found earlier in the MRCI calculations, the barrier at the CCSD(T)/CBS level is largely insensitive to the level at which the geometry of the transition state is optimized. For instance, classical (i.e., not zero-point corrected) CCSD(T)/CBS barriers calculated using geometries obtained at the MP2/aug-cc-pvdz,

TABLE 2: Calculated Characteristic Geometrical Parameters of the Transition State in the O + CH_4 → OH + CH_3 Reaction[a]

	R(OH)/Å	R(CH)/Å	∠OHC/deg	ω_i/cm^{-1}
B3LYP/adz	1.201	1.323	179.4	1396
B3LYP/atz	1.199	1.319	179.4	1448
MP2/adz	1.222	1.265	179.1	2197
MP2/atz	1.222	1.251	179.1	2222
CCSD/adz	1.202	1.317	179.3	1990
CCSD(T)/adz	1.202	1.317	179.2	1885

[a] R(O−H) is the length of the bond that is forming; R(C−H) is the length of the bond that is breaking; ∠O−H−C is the angle between the forming and breaking bond; ω_i is the imaginary frequency at the transition state.

MP2/aug-cc-pvtz, B3LYP/aug-cc-pvdz, and B3LYP/aug-cc-pvtz levels differ by less than 0.1 kcal/mol. This result indicates that either all of the four lower-level methods predict very similar transition-state geometries or that the CCSD(T) energies are somewhat insensitive to the geometries of the transition state. To shed light on this issue, we show in Table 2 characteristic geometrical parameters of the O + CH_4 transition state calculated at different levels of theory. All of the methods predict a similar angle between the breaking and forming bonds (quasicollinear), and a similar bond length for the forming bond (O−H, ∼1.2 Å). However, the methods differ somewhat for the C−H breaking bond. In particular, we see that MP2 predicts a C−H distance notably shorter (∼0.05 Å) than B3LYP and CCSD, which agree with each other. Although B3LYP and CCSD transition-state geometries seem to agree, there is a large discrepancy in the transition-state imaginary frequencies (Table 2). The imaginary frequency at the B3LYP level is notably smaller than the CCSD one, indicating that the B3LYP minimum-energy reaction path is much less sharply peaked in the transition-state region than predicted by CCSD. The imaginary frequency at the MP2 level is larger than the CCSD one, but the deviations from CCSD are smaller than with B3LYP. Regardless, we see that slightly different transition-state geometries provide very similar barriers in CCSD(T)/CBS dual-level calculations.

We now turn our attention to the performance of electronic structure methods of lower cost than CCSD(T) and MRCI. MP2/CBS calculations underestimate the CCSD(T)/CBS reaction endothermicity by approximately 1 kcal/mol and overestimate the CCSD(T) barrier by more than 2 kcal/mol. Spin-projected[22] MP2 calculations extrapolated to the complete basis-set limit (PMP2/CBS) notably improve upon the regular MP2 calculations and provide a reaction barrier within ∼0.5 kcal/mol of the CCSD(T) results. Although these PMP2 calculations reproduce remarkably well the reaction barrier, they predict reaction energies more than 2 kcal/mol below the CCSD(T) data. MP4/CBS calculations reduce the deviation of MP2/CBS data with respect to CCSD(T) in the reaction barrier from over 2 kcal/mol to about 1 kcal/mol. In addition, the MP4/CBS reaction energy matches quite accurately the CCSD(T) data. The spin-projected MP4 barrier (PMP4/CBS) is similar to the PMP2/CBS result, but the error in the reaction energy is decreased from over 2 kcal/mol to less than 1 kcal/mol. Finally, B3LYP/CBS calculations underestimate the reaction energy by over 2 kcal/mol, and the reaction barrier by as much as 5 kcal/mol.

Taking into consideration the description of both the reaction energy and barrier in comparison with MRCI or CCSD(T) data, we can establish a hierarchy of accuracy of the lower-level methods explored in this work for the O(^{3}P) + CH_4 reaction, in terms of decreasing accuracy: PMP4 > MP4 > PMP2 > MP2 > B3LYP. Interestingly, if we focus only on the description of the barrier, the sequence of methods is as follows: PMP2 ≈ PMP4 > MP2 ≈ MP4 > B3LYP. This result is important because PMP2 calculations require a much smaller computational expenditure than PMP4 and can therefore be applied to systems for which CCSD(T) or even PMP4 calculations are prohibitive.

TABLE 3: Calculated Barrier and Reaction Energy (kcal/mol) of the O + C_2H_6 → OH + C_2H_5 Reaction

method	$\Delta H^{\ddagger}$ [a]	$\Delta E^{\ddagger}$ [b]	$\Delta_r H$ [c]	$\Delta_r E$ [d]
CCSD(T)/CBS//MP2/adz	6.90	10.66	−2.58	1.53
CCSD(T)/CBS[e]//MP2/adz	7.00	10.76	−2.53	1.58
MP2/CBS//MP2/adz	9.87	13.63	−3.04	1.07
PMP2/CBS//MP2/adz	7.15	10.91	−4.54	−0.43
CASPT2/CBS[e]//CASPT2/tz	5.3	9.3	−4.6	−0.5
MRCI+Q/CBS[e]//CASPT2/tz	9.0	13.0	−1.4	2.7
exp[23] (0 K)			−5.5 ± 1.4	
exp[23] (298 K)			−5.0 ± 1.4	
exp[24] (298 K)			−1.7 ± 0.4	
exp[25] (298 K)			−1.3	
exp[26] (298 K)			−2.2	

[a] Zero-point corrected transition-state energy referred to reagents. [b] Classical, i.e., not zero-point corrected transition-state energy referred to reagents. [c] Zero-point corrected reaction energy. [d] Classical, i.e., not zero-point corrected reaction energy. [e] The extrapolation to the basis set limit has been performed with the cc-pVTZ and cc-pVQZ basis sets, i.e., without including diffuse functions, ref 20.

In the following, we investigate the barrier of hydrogen abstraction from longer-chain alkanes by O(^{3}P). Since dual-level calculations of the reaction energies and barriers seem insensitive to the level at which the geometry of the pertinent species is optimized, we choose to carry out geometry optimizations and frequency calculations at the MP2/aug-cc-pvdz level from now on.

(b) O(^{3}P) + Ethane. Table 3 shows calculations of the O + C_2H_6 → OH + C_2H_5 reaction energetics at different levels of theory. First, we note that there is a sizable disparity between various experimental reaction energies at 298 K.[23−26] In particular, the reaction energy obtained from the heats of formation of the reagent and product species provided by the Computational Chemistry Comparison and Benchmark Database[23] is ∼3 kcal/mol lower than the rest of the experimental sources used here. Neglecting this result, the average reaction energy of the rest of the experimental measurements is ∼−1.7 kcal/ mol at 298 K and ∼−2.3 kcal/mol at 0 K. Both MRCI/CBS and CCSD(T)/CBS results are within 1 kcal/mol of this experimental average, although CCSD(T) seems to be closer to experiment. On the other hand, CASPT2/CBS calculations overestimate the reaction exothermicity by over 2 kcal/mol. The performance of the cheaper MP2 and PMP2 methods is similar to that in O + methane, with reaction energies approximately 0.5 and 2 kcal/mol more negative than the CCSD(T)/CBS results, respectively.

The differences between the various electronic structure methods examined here are more remarkable for the reaction barrier. CCSD(T)/CBS calculations predict a reaction barrier 2 kcal/mol smaller than that of MRCI/CBS. This is at odds with the results in O + methane, where the deviation between both methods was minimal. The source of this discrepancy seems to lie with the active space used in the MRCI calculations, which included one methyl moiety, but not the other. In effect, Yan et al. predicted that the reaction barrier at 0 K should be 7 ± 1 kcal/mol. They then concluded that the overly large 9 kcal/mol barrier resulting from their MRCI/CBS calculations was probably due to an unbalanced active space.[20] Our CCSD(T)/CBS calculations agree well with the prediction of Yan et al., even

TABLE 4: Calculated Characteristic Geometrical Parameters of the Transition State in the O + C_nH_{2n+2} → OH + C_nH_{2n+1} Reactions at the MP2/aug-cc-pvdz Level[a]

	R(OH)[b]/Å	R(CH)[c]/Å	∠OHC/deg	ω_i/cm^{-1}
Primary Sites				
O + CH_4 (C_s)	1.222	1.265	179.1	2197
O + C_2H_6 (C_s)	1.257	1.244	177.5	2063
O + C_3H_8 (C_s)	1.253	1.246	177.8	2048
O + C_3H_8 (C_1)	1.259	1.245	176.9	2025
O + i-C_4H_{10} (C_s)	1.259	1.248	179.5	2000
O + i-C_4H_{10} (C_1)	1.255	1.246	177.4	2011
O + i-C_5H_{12} (C_1,a)	1.256	1.245	178.4	2039
O + i-C_5H_{12} (C_1,b)	1.256	1.246	178.6	2007
O + i-C_5H_{12} (C_1,c)	1.260	1.247	179.5	1987
O + i-C_5H_{12} (C_1,d)	1.259	1.246	178.9	2013
O + i-C_5H_{12} (C_1,e)	1.258	1.247	173.7	2058
O + i-C_5H_{12} (C_1,f)	1.255	1.247	178.1	2004
O + i-C_5H_{12} (C_1,g)	1.260	1.247	179.6	1996
O + i-C_5H_{12} (C_1,h)	1.256	1.246	175.3	2018
O + i-C_5H_{12} (C_1,i)	1.256	1.246	177.1	2002
Secondary Sites				
O + C_3H_8 (C_s)	1.288	1.228	174.2	1891
O + i-C_5H_{12} (C_1, a)	1.290	1.229	175.1	1845
O + i-C_5H_{12} (C_1, b)	1.290	1.231	176.3	1834
Tertiary Sites				
O + i-C_4H_{10} (C_1)	1.314	1.215	177.6	1696
O + i-C_5H_{12} (C_1)	1.318	1.216	177.2	1806

[a] R(O−H) is the length of the bond that is forming; R(C−H) is the length of the bond that is breaking; ∠O−H−C is the angle between the forming and breaking bond; ω_i is the imaginary frequency. [b] The O−H internuclear distance of the free OH radical is 0.975 Å at the MP2/aug-cc-pvdz level. [c] The C−H internuclear distance in alkane molecules is ∼1.10 Å at the MP2/aug-cc-pvdz level.

though CCSD(T) calculations require substantially less computer time than MRCI. Regarding the rest of the methods used here, MP2/CBS calculations overestimate the CCSD(T)/CBS barrier by 3 kcal/mol. On the other hand, the PMP2 method performs superbly, providing a complete basis-set estimate for the reaction barrier that deviates from the CCSD(T)/CBS result by only 0.25 kcal/mol.

As expected from the relative stability of the methyl and ethyl radicals with respect to the methane and ethane molecules, comparison of the reaction energies of the O + CH_4 → OH + CH_3 and O + C_2H_6 → OH + C_2H_5 reactions indicates that the latter reaction is almost 4 kcal/mol more exothermic. The transition state of the O + ethane abstraction reaction is ∼3 kcal/mol more stable than that in O + methane according to CCSD(T)/CBS calculations. The result that a stabilization of reaction products entails a stabilization of the corresponding transition state concurs with the expectation from Hammond's postulate. Furthermore, the decrease in the reaction barrier when going from the O + methane to the O + ethane reaction is accompanied by a shift of the transition state toward reagents. Table 4 clearly shows that the forming and breaking bonds in the O + ethane reaction transition state are respectively longer and shorter than those in O + methane, i.e., more reactants-like. These findings about the transition-state geometries are also in line with the predictions of Hammond's postulate for O + alkane reactions.

(c) O(^{3}P) + Propane. The O(^{3}P) + C_3H_8 → OH + C_3H_7 reaction is the simplest O + acyclic alkane reaction in which hydrogen abstraction can occur at a secondary site. Another difference with the O + methane and O + ethane reactions studied before is that in O + propane there are two inequivalent primary sites at 0 K. As can be seen in Figure 1, one of the primary sites corresponds to the hydrogen atoms located in the plane of the carbon atoms. The transition state and *n*-propyl radical generated by hydrogen abstraction at this site possess C_s symmetry. The other primary site involves out-of-plane atoms. Therefore, the transition state and *n*-propyl radical in this reaction are not symmetric. Figure 1 also shows the secondary site. The transition state and isopropyl radical corresponding to reaction at the secondary site are C_s-symmetric.

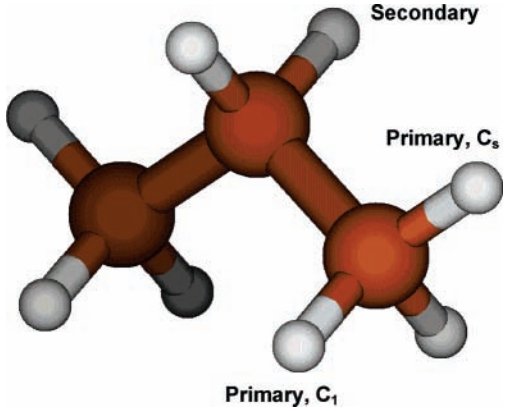

Figure 1. Schematic of the inequivalent hydrogen-abstraction sites in propane.

We could not afford CCSD(T)/aug-cc-pVQZ calculations for this system (the CCSD(T)/aug-cc-pVTZ single-point energy calculation for the asymmetric transition state took 12 days of CPU time). Therefore, CCSD(T)/CBS estimates of the reaction energy and barrier are not provided here. Instead, we use CCSD(T) calculations with the aug-cc-pVTZ basis set to further calibrate the performance of MP2 and PMP2 methods, with which we carry out aug-cc-pVQZ calculations and complete basis-set extrapolations. The zero-point corrected reaction energies of the hydrogen abstractions at the secondary and C_s and C_1 primary sites calculated at the CCSD(T)/aug-cc-pVTZ//MP2/aug-cc-pVDZ level are −3.18, 0.00, and −0.40 kcal/mol, respectively. At the MP2/aug-cc-pVTZ//MP2/aug-cc-pVDZ and PMP2/aug-cc-pVTZ//MP2/aug-cc-pVDZ levels, the same reaction energies are −3.46, −0.44, and −0.87 kcal/mol, and −5.00, −1.92, and −2.35 kcal/mol, respectively. Thus, MP2 energies are within 0.5 kcal/mol of the CCSD(T) results, and PMP2 overestimates CCSD(T) data by ∼2 kcal/mol. The deviations of MP2 and PMP2 from CCSD(T) match those discussed above for O + CH_4 and O + C_2H_6. Regardless of the specific values obtained at each level of theory, all of the methods predict that the reaction at the secondary site is about 3 kcal/mol more exothermic than the average of reaction energies at primary sites with the aug-cc-pVTZ basis set. The calculations also predict that the C_1 *n*-propyl radical is about 0.4 kcal/mol more stable than the C_s counterpart.

Regarding the reaction barriers, the CCSD(T)/aug-cc-pVTZ//MP2/aug-cc-pVDZ zero-point corrected values for the abstraction at the secondary and at the C_s and C_1 primary sites are 4.70, 7.41, and 7.03 kcal/mol, respectively. The same barriers at the MP2 and PMP2 levels are 7.74, 10.27, and 9.93 kcal/mol, and 5.21, 7.55, and 7.23 kcal/mol, respectively. Therefore, as previously reported for O + CH_4 and O + C_2H_6, while the PMP2 barriers are within 0.5 kcal/mol of the CCSD(T) values, MP2 overestimates the higher-level results by ∼3 kcal/mol. An important result predicted by all theories is that the barrier for abstraction at the secondary site is more than 2 kcal/mol smaller than the barrier at the primary sites. This decrease in the barrier agrees with the trend observed in the experimentally determined activation energies.[5] However, a caveat in the experiments is that the activation energy from secondary sites in an acyclic alkane has not been unequivocally determined yet. Instead, the

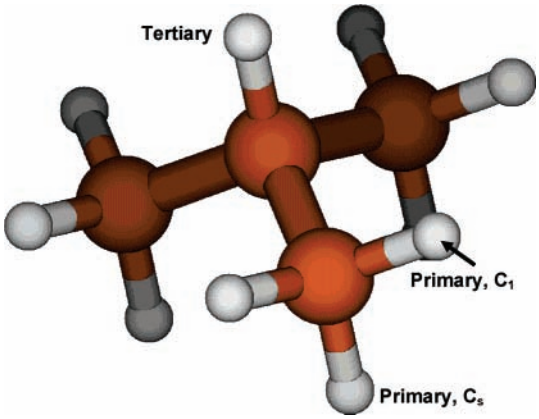

Figure 2. Schematic of the inequivalent hydrogen-abstraction sites in isobutane.

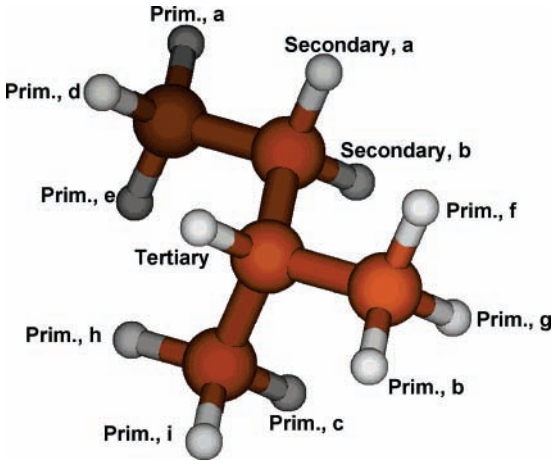

Figure 3. Schematic of the inequivalent hydrogen-abstraction sites in isopentane.

community has been using the activation energy obtained from thermal rate constants in the O + cyclohexane as a model for acyclic secondary sites. The result that the barrier at secondary sites is smaller than at primary sites also highlights that the Hammond's postulate nicely applies to the O + alkane reactions: a stabilization of products (i.e., an increase in the reaction exothermicity) is connected with a stabilization of the transition state (i.e., a decrease in the reaction barrier). Analysis of the transition-state geometries (Table 4) indicates that the stabilization of the transition state in the reaction at the secondary site with respect to the primary sites also entails structural changes in the transition state. For instance, the bonds that are forming (O−H) and breaking (C−H) are respectively 2.5% longer and 1.4% shorter in the transition state for abstraction at the secondary site than at primary sites. In other words, electronic structure calculations predict that the transition state for abstraction at the secondary site is more reagents-like than at primary sites.

(d) O(^{3}P) + Isobutane. The O(^{3}P) + i-C_4H_{10} → OH + C_4H_9 reaction is the simplest O + acyclic alkane reaction in which hydrogen abstraction can occur at a tertiary site. The isobutane molecule does not have secondary hydrogen atoms, and as in propane, there are two dissimilar primary sites of C_s and C_1 symmetry. The symmetry-inequivalent primary and tertiary sites are displayed in Figure 2. Similarly to the lower-dimensionality O + alkane systems reported before, we have carried out CCSD(T) calculations of the reaction energies and barriers and compared them with the estimates of MP2 and PMP2 methods. However, due to the computational overhead of CCSD(T) calculations, we have only been able to use the aug-cc-pVDZ basis set to determine the reaction energies and barrier for this system. The CCSD(T)/aug-cc-pVDZ//MP2/aug-cc-pVDZ zero-point corrected energies of the abstraction at the tertiary and the C_s and C_1 primary sites are −2.26, 1.85, and 2.04 kcal/mol, respectively. The MP2/aug-cc-pvdz and PMP2/aug-cc-pVDZ//MP2/aug-cc-pVDZ estimates for the same reaction energies are −2.53, 1.28, and 1.49 kcal/mol, and −3.95, 0.13, and 0.10 kcal/mol, respectively. As noted earlier, MP2 results are typically within 0.5 kcal/mol of CCSD(T), and PMP2 overestimates the CCSD(T) reaction exothermicity by about 2 kcal/mol. Therefore, the trend seen in the all the previously studied reactions about the relative accuracy of MP2, PMP2, and CCSD(T) is extended to O + isobutane. All three methods indicate that the energy of the reaction at the tertiary site is about 4 kcal/mol below the reaction energy at the primary sites. The MP2 and PMP2 CBS estimates of the reaction energies with geometries and harmonic frequencies obtained at the MP2/aug-cc-pVDZ level are as follows: −6.50, −1.96, and −1.70 kcal/mol and −7.99, −3.43, and −3.18 kcal/mol respectively. Thus, calculations extrapolated to the complete basis-set limit predict that hydrogen abstraction at the tertiary site is ∼4.5 kcal/mol more exothermic than at primary sites. This difference in the reaction exothermicity at the tertiary and primary sites is in good agreement with the difference in the two reaction energies obtained from the corresponding experimental heats of formation at 298 K (5.0 kcal/mol; see ref 27).

The reaction barriers at the CCSD(T)/aug-cc-pVDZ//MP2/aug-cc-pVDZ level are 3.08, 7.47, and 7.81 kcal/mol for the abstractions at the tertiary, primary-C_s, and primary-C_1 sites, respectively. The same barriers at the MP2/aug-cc-pVDZ level are 6.00, 10.18, and 10.42 kcal/mol, and 3.66, 7.48, and 7.71 kcal/mol at the PMP2/aug-cc-pVDZ//MP2/aug-cc-pVDZ level. Again, while MP2 overestimates the CCSD(T) energies by 2.5−3.0 kcal/mol, the PMP2 barriers are within ∼0.5 kcal/mol of the CCSD(T) values.

Complete basis-set estimates of the barriers at the PMP2 level are 3.30, 6.76, and 6.55 kcal/mol for abstraction at the tertiary and C_s and C_1 primary sites. Once again, we see that the most exothermic reaction is tied to the lowest barrier, as predicted by Hammond's postulate. In addition, the transition-state geometries for the tertiary and primary transition states reported in Table 4 show that the tertiary transition state is remarkably more reactant-like than the primary transition states, also in accordance with Hammond's postulate. In effect, the O−H and C−H internuclear distances of the tertiary-site transition state are respectively 4.6% longer and 2.6% shorter than those of the primary-sites transition states.

(e) O(^{3}P) + Isopentane. O(^{3}P) + i-C_5H_{12} is the simplest O + acyclic alkane reaction in which hydrogen abstraction can occur at primary, secondary, and tertiary sites. Therefore, this system is the simplest reduced-dimensionality model of squalane or other hydrocarbon surfaces with accessible primary, secondary, and tertiary sites. A difficulty with the reaction energy and barrier calculations of this system is that the absence of symmetry in the isopentane molecule makes all of the hydrogen atoms inequivalent. Therefore, there are 9 inequivalent primary reactive sites, 2 secondary, and 1 tertiary. We show in Figure 3 all 12 inequivalent reaction sites in the O + i-pentane reaction and the labeling system that we use hereafter.

The fact that we have only observed a ∼0.5 kcal/mol difference between the barriers calculated at PMP2 and CCSD(T) levels in all of the O + alkane systems studied until now suggests that PMP2 should be accurate in determining O + alkane hydrogen-abstraction barriers in larger O + alkane

TABLE 5: Calculated Reaction Barriers, Reaction Energies (kcal/mol), and Thermal (298 K) Rate Constants (cm^3 molecule^{-1} s^{-1}) in O + C_nH_{2n+2} → OH + C_nH_{2n+1} Reactions[a]

	$\Delta H^{\ddagger}$ [b]	$\Delta E^{\ddagger}$ [c]	$\Delta_r H$ [d]	$\Delta_r E$ [e]	k(TST)	k(TST/W)
			Primary Sites			
O + CH_4 (C_s)	9.90	13.93	0.24	4.16	6.18×10^{-19}	3.52×10^{-18}
O + C_2H_6 (C_s)	7.15	10.91	−3.04	1.07	2.55×10^{-17}	13.1×10^{-17}
O + C_3H_8 (C_s)	7.23	10.98	−2.06	1.77	1.89×10^{-17}	9.61×10^{-17}
O + C_3H_8 (C_1)	6.93	10.57	−2.52	1.44	2.53×10^{-17}	12.6×10^{-17}
O + i-C_4H_{10} (C_s)	6.77	10.42	−1.96	1.88	2.56×10^{-17}	12.5×10^{-17}
O + i-C_4H_{10} (C_1)	6.55	10.20	−1.70	2.17	4.67×10^{-17}	23.1×10^{-17}
O + i-C_5H_{12} (C_1,a)	6.75	10.78	−2.77	1.22	7.47×10^{-17}	37.7×10^{-17}
O + i-C_5H_{12} (C_1,b)	6.98	10.60	−2.02	1.81	1.85×10^{-17}	9.10×10^{-17}
O + i-C_5H_{12} (C_1,c)	6.65	10.33	−2.06	1.77	3.38×10^{-17}	16.4×10^{-17}
O + i-C_5H_{12} (C_1,d)	6.85 [f]	10.54	−2.93	1.06	2.46×10^{-17}	12.2×10^{-17}
O + i-C_5H_{12} (C_1,e)	7.48	11.11	−2.93	1.06	0.67×10^{-17}	3.41×10^{-17}
O + i-C_5H_{12} (C_1,f)	7.04	10.67	−2.02	1.82	1.97×10^{-17}	9.67×10^{-17}
O + i-C_5H_{12} (C_1,g)	6.71	10.37	−2.02	1.82	2.83×10^{-17}	13.8×10^{-17}
O + i-C_5H_{12} (C_1,h)	6.93	10.49	−2.00	1.84	1.37×10^{-17}	6.80×10^{-17}
O + i-C_5H_{12} (C_1,i)	6.96	10.63	−2.00	1.84	2.25×10^{-17}	11.0×10^{-17}
			Secondary Sites			
O + C_3H_8 (C_s)	4.98	8.67	−5.28	−1.21	9.16×10^{-16}	4.10×10^{-15}
O + i-C_5H_{12} (C_1,a)	4.66 [g]	8.29	−4.60	−0.83	8.85×10^{-16}	3.82×10^{-15}
O + i-C_5H_{12} (C_1,b)	4.61	8.23	−4.60	−0.83	9.15×10^{-16}	3.91×10^{-15}
			Tertiary Sites			
O + i-C_4H_{10} (C_1)	3.31	7.05	−6.50	−2.78	1.92×10^{-14}	7.30×10^{-14}
O + i-C_5H_{12} (C_1)	3.24	6.80	−5.97	−2.42	1.00×10^{-14}	4.18×10^{-14}

[a] The barriers have been calculated at the PMP2/CBS//MP2/aug-cc-pvdz level, and the reaction energies show MP2/CBS//MP2/aug-cc-pvdz calculations. The symmetry labels refer to the symmetries of the transition states. [b] Zero-point corrected transition-state energy referred to reagents. [c] Classical, i.e., not zero-point corrected transition-state energy referred to reagents. [d] Zero-point corrected reaction energy. [e] Classical, i.e., not zero-point corrected reaction energy. [f] An instability in the orbital Hessian for this transition-state structure yielded one unphysical normal-mode frequency. Therefore, the zero-point correction for this barrier was taken to be the average of the other eight primary barriers. [g] An instability in the orbital Hessian for this transition-state structure yielded one unphysical normal-mode frequency. Therefore, the zero-point correction for this barrier was taken directly from the other secondary barrier.

systems. Therefore, instead of conducting overly expensive CCSD(T) calculations for the 12 transition states of the O + isopentane reaction, we have used more affordable PMP2 calculations, which are expected to provide energy barriers within 0.5 kcal/mol of the CCSD(T) values.

Table 5 shows that the reaction energies for abstraction of the 9 dissimilar primary hydrogen atoms calculated at the MP2/CBS//MP2/aug-cc-pVDZ level are within 1 kcal/mol of each other. We note that the reaction energies for abstraction are identical in the d−e, f−g, and h−i pairs of reactions because the geometry optimizations of these primary alkyl radical pairs converged to the same structure. The same behavior was observed in geometry optimizations of the secondary alkyl radicals generated from hydrogen abstraction of the two dissimilar secondary hydrogen atoms. Regardless, we see that on average, hydrogen abstraction at secondary sites in isopentane is ∼2.5 kcal/mol more exothermic than at primary sites. Moreover, abstraction at the tertiary site is ∼1.5 kcal/mol more exothermic than at secondary sites.

Regarding the reaction barriers, PMP2/CBS//MP2/aug-cc-pVDZ calculations predict that the average barrier for hydrogen abstraction at primary sites is 6.93 kcal/mol. All 9 primary abstraction barriers are within 0.6 kcal/mol of this average. The average of the two secondary barriers is 4.64 kcal/mol, with both barriers being within 0.05 kcal/mol of this value. The barrier height for abstraction at the tertiary site, 3.24 kcal/mol, is ∼1.4 and ∼3.7 kcal/mol smaller than the average barriers at secondary and primary sites, respectively.

The trends in the reaction energies and barriers of different alkane sites in the O(^{3}P) + i-C_5H_{12} → OH + i-C_5H_{11} reaction add to the wealth of evidence that supports the suitability of Hammond's postulate for O + alkane reactions. The hydrogen abstraction reaction becomes more exothermic in the primary → secondary → tertiary order. The increase in exothermicity is accompanied by a decrease in the reaction barrier in that same order and by a shift in the geometry of the transition state toward an increasingly reactant-like structure also in that order (see Table 4).

IV. Discussion

Using the ab initio reaction energies, barriers, and transition-state geometries reported above, we now examine the trends across the various O + alkane systems investigated in this work. Our goals are to provide a sensible estimate of relative reactivity of primary, secondary, and tertiary sites in O + alkane reactions involving longer-chain gas-phase and condensed-phase alkanes. We also aim at substantiating the legitimacy of the often-invoked Hammond's postulate for these reactions.

Table 5 shows the reaction barriers calculated at the highest level of theory that we have been able to afford in all reactions investigated in this work (PMP2/CBS). Regarding the barriers for abstraction at primary sites, we note that there is a strong difference between methane and the rest of hydrocarbons, with the barrier in methane (9.90 kcal/mol) being about 3 kcal/mol higher than the average of the rest of the barriers for abstraction at primary sites (6.93 kcal/mol). This result indicates that caution must be used when employing methane as a reduced-dimensionality model for abstraction at primary sites. The barriers for abstraction at primary sites in ethane, propane, isobutane, and isopentane (14 barriers overall) are within 1 kcal/mol of each other. Furthermore, the averages of the primary barriers for each alkane studied (7.15, 7.08, 6.66, and 6.93 kcal/mol for ethane, propane, isobutane, and isopentane, respectively) deviate by less than 0.3 kcal/mol from the average of all 14 symmetry-inequivalent primary barriers (6.93 kcal/mol). The close proximity of the primary barriers suggests that the molecules chosen in this study suffice to capture the value of

the primary hydrogen-abstraction barrier in O + alkane reactions other than O + methane.

Regarding abstraction at secondary sites, we show in Table 5 that the 3 symmetry-inequivalent barriers studied in this work are within 0.3 kcal/mol of each other and deviate by less than 0.15 kcal/mol from their average (4.75 kcal/mol). The similarity of the barrier heights at secondary sites in the O + propane and O + isobutane reactions suggests that the average barrier height calculated here is representative of the barrier at secondary sites in longer-chain or condensed-phase acyclic alkanes. The two barriers for hydrogen abstraction at tertiary sites calculated here (3.31 kcal/mol in isobutane and 3.24 kcal/mol in isopentane) are within 0.07 kcal/mol of each other. It is therefore likely that the average of these barriers (3.28 kcal/mol) is also a good representation of the barrier in larger acyclic alkanes.

A direct comparison of the average barriers for hydrogen abstraction by oxygen atoms at primary, secondary, and tertiary sites (6.93, 4.75, and 3.28 kcal/mol at the PMP2/aug-cc-pvdz level) substantiates the previously estimated ordering of the barriers in the primary > secondary > tertiary sequence. This decrease in the barriers is accompanied by an evolution in the transition-state geometry toward reagents in the same order. For instance, the average length of the bond that is forming (O−H) becomes increasingly longer in the primary → secondary → tertiary sequence (1.257 Å in primary transition states (except methane), 1.290 Å in secondary transition states, and 1.316 Å in tertiary transition states). Meanwhile, the average breaking-bond length (C−H) becomes shorter in that same sequence (1.246, 1.229, and 1.216 Å for primary (except methane), secondary, and tertiary transition states). Further information about the changes in the minimum-energy reaction path of reactions at primary, secondary, and tertiary sites can be gleaned from the values of the imaginary frequencies at the transition state. Table 4 shows that the imaginary frequencies decrease in the primary → secondary → tertiary order, implying a flattening of the reaction path at the transition state in that order. This flattening bodes well with the lower reaction barrier and the shift of the transition state toward reagents discussed above.

Using the geometries, harmonic frequencies, and energies of reagents and transition states, we have calculated the thermal rate constants at room temperature (298 K) for each of the reactions studied here via transition-state theory (TST). Tunneling has been estimated using the Wigner method (TST/W). Both sets of rates are shown in Table 5. Leaving aside O + methane, the average rate constants (including tunneling) for abstraction at primary sites in each O + alkane system (1.31×10^{-16}, 1.11×10^{-16}, 1.78×10^{-16}, and 1.33×10^{-16} cm^3 $molecule^{-1}$ s^{-1} for ethane, propane, isobutane, and isopentane) are within 30% of the overall average rate constant at primary sites (1.36×10^{-16} cm^3 $molecule^{-1}$ s^{-1}). The average tunneling-corrected rate constant at secondary sites is 3.94×10^{-15} cm^3 $molecule^{-1}$ s^{-1}, with the individual rate constants deviating less than 5% from that average. Finally, the average TST/W rate constant at tertiary sites is predicted to be 5.74×10^{-14} cm^3 $molecule^{-1}$ s^{-1}. These rates indicate that the average room-temperature relative reactivity of primary, secondary, and tertiary sites in reactions of atomic oxygen with acyclic alkanes is 1:29:422.

A way to assess the accuracy of these relative reactivities is to compare the absolute thermal rate constants obtained from the PMP2/CBS calculations via transition-state theory with experiments. Here we choose to compare the calculated rate constants for O + ethane, O + propane, and O + isobutane with experiment to test the accuracy of the calculations for primary, secondary, and tertiary sites. The calculated room-temperature (298 K) thermal rate constants for O + C_2H_6, O + C_3H_8, and O + i-C_4H_{10} (0.78×10^{-15}, 8.9×10^{-15}, and 0.75×10^{-13} cm^3 $molecule^{-1}$ s^{-1}, respectively) are in quite good agreement with the experimental results[27] (1.1×10^{-15}, 6.6×10^{-15}, and 1.2×10^{-13} cm^3 $molecule^{-1}$ s^{-1}, respectively). The calculated values are well within a factor of 2 of the measurements. This level of agreement is typical of conventional transition-state theory with Wigner tunneling correction using accurate barriers. The satisfactory comparison between experimental and theoretical rate constants therefore lends confidence to the calculated relative reactivities reported above for primary, secondary, and tertiary sites.

As mentioned before, in the absence of selective isotopic labeling, experiments measuring the internal-state distribution of the OH product generated in collisions of O with liquid squalane cannot determine directly the type of hydrogen atom abstracted.[9−11] The presence of vibrationally excited OH suggests that some of the hydrogen atoms might be abstracted from secondary or even tertiary sites. Molecular dynamics and Monte Carlo simulations of the interfacial structure of squalane support this idea by revealing that secondary and tertiary sites are exposed to collisions with incoming oxygen atoms.[12] With this information in mind, we now use the calculations performed in this work to provide quantitative insight into the possibility that secondary and tertiary sites contribute to the reactivity of squalane in collisions with O atoms. The relative contributions of the various squalane sites to the total OH yield in thermal O + squalane reactions can be determined by multiplying the relative room-temperature rates for primary, secondary, and tertiary sites by the relative abundances of these sites in squalane (24, 32, and 6, respectively). Thus, the relative reactivities of each site weighted by their abundances are 1:39:106 for primary:secondary:tertiary sites. These results indicate that if primary, secondary, and tertiary sites in squalane are equally exposed to incoming O atoms, the total OH yield will be dominated by reaction at secondary and tertiary sites.

A caveat in using room-temperature thermal rate constants to provide insight into the experiments of McKendrick and coworkers is that the incoming O atoms are not thermal in the experiments.[9−11] Instead, O(^{3}P) is generated by NO_2 photodissociation at 355 nm. This photolysis process produces O(^{3}P) with a very broad distribution of superthermal collision energies, characterized by an average energy of 3.8 kcal/mol and a full width at medium height of 6.2 kcal/mol. Comparison of the experimental collision energy with the barriers in Table 5 indicates that only the barrier for hydrogen abstraction at tertiary sites is below the average experimental collision energy. The barrier for abstraction at secondary sites is slightly larger than the average collision energy. Thus, if the collision-energy distribution is symmetric, less than half of the collisions will have enough energy to surmount the abstraction barrier at secondary sites. The average barrier for abstraction at primary sites (6.9 kcal/mol) is more than 3 kcal/mol larger than the average experimental collision energy. Therefore, reaction at these sites is only possible with the high-energy tail of the collision-energy distribution provided by NO_2 photolysis. Two main reaction mechanisms are expected to contribute to the total OH yield in O + squalane reactions. In collisions following the Eley−Rideal mechanism, the impinging O atoms will react directly with exposed hydrogen atoms. This mechanism is analogous to direct gas-phase reactions. On the other hand, in collisions undergoing the Hinshelwood−Langmuir mechanism,

the incoming oxygen atoms thermally accommodate on the surface via inelastic collisions before reaction. If the reactions occur following the Hinshelwood−Langmuir mechanism, the relative rates provided in this work should capture accurately the contributions of primary, secondary, and tertiary sites to the total OH yield. Even if the reaction is direct (Eley−Rideal mechanism) and the thermal reactivities predicted cannot be used directly, the comparisons between experimental collision energy and barriers noted above indicate that the contribution from secondary and tertiary sites to the total OH yield will be sizable.

Our calculations can also be used to provide information about the energy disposal into the products' degrees of freedom. As mentioned earlier, the measured increase in OH vibrational excitation in the primary → secondary → tertiary reaction-site sequence is well-captured by the ab initio shift in the geometry of transition state toward reagents in that order. We now focus on providing an estimate for the internal excitation of the alkyl radical. Recently, measurements of energy release to the alkyl radical in $O(^3P)$ + alkane reactions by Suits and co-workers have been interpreted using Franck−Condon-like arguments.[28] The interpretation states that if the hydrogen-abstraction reaction is sudden, then the reorganization energy of the alkyl fragment when going from the transition state to products appears as vibrational excitation in the alkyl product. In other words, the energy released by the change in geometry of the alkyl radical during the reaction is not shared by the rest of the products' degrees of freedom. Instead, that energy remains in the alkyl product. This argument has been recently applied to understand alkyl product internal excitation in the $F + C_2H_6 \rightarrow HF + C_2H_5$ reaction.[29] If the argument that hydrogen abstraction is sudden and the energy released by the alkyl fragment in the geometry relaxation from the transition state to products stays in the alkyl fragment indeed applies, we can use our calculations to predict the extent of alkyl excitation as a function of the abstraction site.

For this purpose, we have calculated the difference in energy between the alkyl radicals at their geometry in reagents or the transition state and the geometry in products. Extensive calculations for the O + methane and ethane reactions indicate that this difference in energy is quite insensitive to the method of calculation and basis set, so the data we show here have been calculated at the MP2/aug-cc-pvdz level. We present results for the largest reaction studied in this work ($O(^3P)$ + i-pentane), as we have demonstrated that this system is representative of general O + alkane reactions at primary, secondary, and tertiary sites. The average relaxation energies of the primary, secondary, and tertiary alkyl fragments when going from reagents to products are 6.49, 5.97, and 5.27 kcal/mol, respectively. We note that there is good agreement between our result for secondary alkyl radicals and that calculated by Suits and co-workers in the 2-butyl radical (5.6 kcal/mol).[28] If this relaxation energy is maintained as alkyl internal energy in products, then abstractions at primary sites should promote more excitation in the alkyl product than at secondary and tertiary sites. Calculation of the alkyl energy at the transition-state geometry allows one to obtain the relaxation energy from the transition state to products. The average alkyl relaxation energies from the transition state to products in the $O(^3P)$ + i-pentane reaction are 2.94, 2.63, and 2.07 kcal/mol respectively for the reaction at primary, secondary, and tertiary sites. Therefore the trend that alkyl excitation in products is increased in the tertiary → secondary → primary sequence applies irrespective of whether the reorganization energy is calculated from reagents or the transition state.

V. Concluding Remarks

We have investigated the reaction energy and barriers of the hydrogen-abstraction reactions between ground-state oxygen atoms and acyclic alkane molecules using electronic structure methods. These calculations have enabled us to quantify accurately the different reactivity of primary, secondary, and tertiary sites of acyclic alkane molecules and provide insight into recent experiments investigating reactions between $O(^3P)$ and liquid alkanes.

Our ab initio studies indicate that spin-projected MP2 results reproduce to within 0.5 kcal/mol all of the reaction barriers calculated in this work with the more accurate CCSD(T) method. This result enables us to use PMP2 as a predictive tool to O + alkane hydrogen-abstraction reaction barriers for which CCSD(T) calculations are prohibitive. Regular MP2 calculations provide a similar comparison with CCSD(T) calculations in the reaction energy.

The calculations in this work substantiate the long-anticipated trend that the reaction barriers in O + acyclic alkane hydrogen-abstraction reactions are in the primary > secondary > tertiary order. Furthermore, the calculations also support the Hammond's postulate prediction that the transition-state structure should become increasingly reagents-like in the primary → secondary → tertiary sequence.

We also learn that the energy barriers for hydrogen abstraction in primary sites of ethane, propane, isobutane, and isopropane are very close to each other. Therefore, an average of these barriers is likely a good estimate of the reaction at primary sites in larger acyclic alkanes. A similar conclusion can be extracted from the calculated barriers at secondary and tertiary sites.

Using our highest-level ab initio data, we have computed the thermal rate constants for hydrogen abstraction at primary, secondary, and tertiary alkane sites by $O(^3P)$ to aid in the understanding of recent experiments on O + squalane. The results indicate that if primary, secondary, and tertiary sites in the surface of squalane are exposed to incoming oxygen atoms as determined by their abundances, reactions at secondary and tertiary sites should dominate over reactions at primary sites under thermal conditions. Even at the superthermal conditions of the recent experiments, reactions at secondary and tertiary sites are expected to provide a major contribution to the total OH yield.

Acknowledgment. This work has been supported by NSF Grant No. CHE-0547543 and AFOSR Grant No. FA9550-06-1-0165. D.T. is a Cottrell Scholar of Research Corporation.

References and Notes

(1) Herron, J. T.; Huie, R. E. *J. Phys. Chem.* **1969**, *73*, 3327.
(2) Hammond, A. S. *J. Am. Chem. Soc.* **1955**, *77*, 334.
(3) Andresen, P.; Luntz, A. C. *J. Chem. Phys.* **1980**, *72*, 5842.
(4) Sweeney, G. M.; Watson, A.; McKendrick, K. G. *J. Chem. Phys.* **1997**, *106*, 9172.
(5) Ausfelder, F.; McKendrick, K. G. *Prog. React. Kinet. Mech.* **2000**, *25*, 299.
(6) Garton, D. J.; Minton, T. K.; Alagia, M.; Balucani, N.; Casavecchia, P.; Volpi, G. G. *J. Chem. Phys.* **2000**, *112*, 5975.
(7) Zhang, J.; Garton, D. J.; Minton, T. K. *J. Chem. Phys.* **2003**, *117*, 6239.
(8) Zhang, J.; Upadhyaya, H. P.; Brunsvold, A. L.; Minton, T. K. *J. Phys. Chem. B* **2006**, *110*, 12500.
(9) Kelso, H.; Kohler, S. P. K.; Henderson, D. A.; McKendrick, K. G. *J. Chem. Phys.* **2003**, *119*, 9985.
(10) Köhler, S. P. K.; Allan, M.; Kelso, H.; Henderson, D. A.; McKendrick, K. G. *J. Chem. Phys.* **2005**, *122*, 024712.
(11) Köhler, S. P. K.; Allan, M.; Costen, M. L.; McKendrick, K. G. *J. Phys. Chem. B* **2006**, *110*, 2771.

(12) Köhler, S. P. K.; Reed, S. K.; Westacott, R. E.; McKendrick, K. G. *J. Phys. Chem. B* **2006**, *110*, 11717.

(13) Halkier, A.; Helgaker, T.; Jorgensen, P.; Klopper, W.; Koch, H.; Olsen, J.; Wilson, A. K. *Chem. Phys. Lett.* **1998**, *286*, 243.

(14) Frisch, M. J.; Trucks, G. W.; Schlegel, H. B.; Scuseria, G. E.; Robb, M. A.; Cheeseman, J. R.; Montgomery, J., J. A.; Vreven, T.; Kudin, K. N.; Burant, J. C.; Millam, J. M.; Iyengar, S. S.; Tomasi, J.; Barone, V.; Mennucci, B.; Cossi, M.; Scalmani, G.; Rega, N.; Petersson, G. A.; Nakatsuji, H.; Hada, M.; Ehara, M.; Toyota, K.; Fukuda, R.; Hasegawa, J.; Ishida, M.; Nakajima, T.; Honda, Y.; Kitao, O.; Nakai, H.; Klene, M.; Li, X.; Knox, J. E.; Hratchian, H. P.; Cross, J. B.; Bakken, V.; Adamo, C.; Jaramillo, J.; Gomperts, R.; Stratmann, R. E.; Yazyev, O.; Austin, A. J.; Cammi, R.; Pomelli, C.; Ochterski, J. W.; Ayala, P. Y.; Morokuma, K.; Voth, G. A.; Salvador, P.; Dannenberg, J. J.; Zakrzewski, V. G.; Dapprich, S.; Daniels, A. D.; Strain, M. C.; Farkas, O.; Malick, D. K.; Rabuck, A. D.; Raghavachari, K.; Foresman, J. B.; Ortiz, J. V.; Cui, Q.; Baboul, A. G.; Clifford, S.; Cioslowski, J.; Stefanov, B. B.; Liu, G.; Liashenko, A.; Piskorz, P.; Komaromi, I.; Martin, R. L.; Fox, D. J.; Keith, T.; Al-Laham, M. A.; Peng, C. Y.; Nanayakkara, A.; Challacombe, M.; Gill, P. M. W.; Johnson, B.; Chen, W.; Wong, M. W.; Gonzalez, C.; Pople, J. A. *Gaussian 03*, Revision C.02; Gaussian Inc.: Wallingford, CT, 2004.

(15) Crawford, T. D.; Sherrill, C. D.; Valeev, E. F.; Fermann, J. T.; King, R. A.; Leininger, M. L.; Brown, S. T.; Janssen, C. L.; Seidl, E. T.; Kenny, J. P.; Allen, W. D. PSI 3.2; 2003.

(16) Corchado, J. C.; Espinosa-Garcia, J.; Roberto-Neto, O.; Chuang, Y.-Y.; Truhlar, D. G. *J. Phys. Chem. A* **1998**, *102*, 4899.

(17) Gonzalez, M.; Hernando, J.; Millan, J.; Sayos, R. *J. Chem. Phys.* **1999**, *110*, 7326.

(18) Roberto-Neto, O.; Machado, F. B. C.; Truhlar, D. G. *J. Chem. Phys.* **1999**, *111*, 10046.

(19) Troya, D.; Pascual, R. Z.; Schatz, G. C. *J. Phys. Chem. A* **2003**, *107*, 10497.

(20) Yan, T.; Hase, W. L.; Doubleday, C. *J. Chem. Phys.* **2004**, *120*, 9253.

(21) Troya, D.; Garcia-Molina, E. *J. Phys. Chem. A* **2005**, *109*, 5814.

(22) Schlegel, H. B. *J. Phys. Chem.* **1988**, *92*, 3075.

(23) Computational Chemistry Comparison and Benchmark Database, http://srdata.nist.gov/cccbdb/.

(24) Experimental reaction energy determined from the heats of formation at 298 K reported in: *Chemical Kinetics and Photochemical Data for Use in Atmospheric Studies*, Evaluation No. 15, JPL Publication 06-2; Jet Propulsion Laboratory: Pasadena, CA, 2006; http://jpldataeval.jpl.nasa.gov/pdf/JPL_15_AllInOne.pdf.

(25) Experimental reaction energy determined from the heats of formation at 298 K reported in: http://www.iupac-kinetic.ch.cam.ac.uk/Thermo2003.pdf.

(26) Experimental reaction energy determined from the heats of formation at 298 K reported in: *NIST Chemistry WebBook*; NIST Standard Reference Database No. 69; Linstrom, P. J., Mallard, W. G., Eds.; National Institute of Standards and Technology: Gaithersburg, MD, June 2005; http://webbook.nist.gov/chemistry/.

(27) Cohen, N.; Westberg, K. R. *J. Phys. Chem. Ref. Data* **1991**, *20*, 1211.

(28) Liu, X.; Gross, R. L.; Hall, G. E.; Muckerman, J. T.; Suits, A. G. *J. Chem. Phys.* **2002**, *117*, 7947.

(29) Whitney, E. S.; Zolot, A. M.; McCoy, A. B.; Francisco, J. S.; Nesbitt, D. J. *J. Chem. Phys.* **2005**, *122*, 124310.